Journal of Applied Polymer Science

Structure and properties of poly(lactic acid)/poly(ε-caprolactone) nanocomposites with kinetically induced nanoclay location

J. Urquijo,[1] S. Dagréou,[2] G. Guerrica-Echevarría,[1] J. I. Eguiazábal[1]

[1]Polymer Science and Technology Department, University of the Basque Country UPV/EHU. Paseo Manuel de Lardizabal 3, 20018, San Sebastián, Spain

[2]Equipe De Physique Et Chimie Des Polymères, 2 Avenue Du Président Angot, Université De Pau Et Des Pays De L'Adour/CNRS IPREM UMR5254, Pau, 64053, France

Correspondence to: J. I. Eguiazábal (E-mail: josei.eguiazabal@ehu.es)

ABSTRACT: Poly(lactic acid)/poly(ε-caprolactone)/organically modified montmorillonite (PLA/PCL/OMMT) nanocomposites were melt-processed in a twin-screw extruder under high shear conditions. As a result of the processing conditions employed, the OMMT layers located in the less compatible PCL phase in all the ternary nanocomposites. The morphology of the PLA/PCL blend evolved from "sea-island" to co-continuous upon the addition of OMMT. Both the X-ray diffraction (XRD) and viscoelastic characterization suggested similar OMMT dispersion in the reference PLA binary and in the PLA/PCL ternary nanocomposites, regardless of its location in the PLA and PCL phase, respectively. The reinforcing effect of the organoclay was also similar. The addition of OMMT to the PLA/PCL blend fully compensated the loss in stiffness and oxygen barrier performance produced by PCL in PLA; the nanocomposite with 3% OMMT showed the same modulus and permeability values as those of pure PLA. Moreover, the ductile behavior (elongation at break $>80\%$) of the PLA/PCL blend remained constant even in the nanocomposite containing 5% OMMT. © 2016 Wiley Periodicals, Inc. J. Appl. Polym. Sci. **2016**, *133*, 43815.

KEYWORDS: biopolymers and renewable polymers; morphology; nanoparticles; properties and characterization; structure-property relations

Received 25 February 2016; accepted 22 April 2016

DOI: 10.1002/app.43815

INTRODUCTION

The challenging issues of diminishing petroleum reserves and disposal and treatment of plastic waste have led to the study and research of new materials based on bio-sourced and/or biodegradable polymers becoming one of the most topical and interesting fields in macromolecular science and technology today. Poly(lactic acid) (PLA), which is 100% bio-sourced and biodegradable has become the most promising biopolymer to date. PLA combines thermoplasticity, optimum stiffness, and strength and can therefore be used to replace conventional polymers in the manufacturing of a wide range of products. Unfortunately, however, PLA also presents some shortcomings, such as its intrinsic brittleness, which considerably limits the range of potential applications, which is why it has frequently been modified in an effort to achieve more balanced properties.

From a mechanical point of view, melt-processed poly(lactic acid)/poly(ε-caprolactone) (PLA/PCL) blends look very promising, since they combine the stiffness of PLA with the deformability of PCL. Additionally, PLA/PCL blends are fully biodegradable. Despite being fully immiscible blends, they have been listed as compatible[1,2] or easily compatibilized,[3,4] and consequently, they present well-balanced mechanical properties. The morphology of PLA-rich compositions, in which even submicron PCL particles can be found finely dispersed within the PLA-matrix, allows an efficient matrix/dispersed-phase stress transfer, and therefore mechanically favorable behavior.

To date, binary polymer blends and nanocomposites have been widely used to develop a broad range of quality polymeric materials. The addition of nanofillers to polymer blends goes one step further, as it produces new materials by combining both technologies. The characteristics of the final ternary nanocomposites are directly associated with the degree of filler dispersion, the location of the nanofillers within the system, and their potential to modify the morphology of the starting polymer blend. The location of the nanofillers is usually established by the chemical affinity between the different system constituents.[5,6] However, under nonequilibrium processing conditions, kinetic effects, such as the blending sequence employed,[7,8] must be considered as factors which may affect the location of the nanofiller in any of the separated polymer phases.[6] The location

of the fillers is of prime importance because it usually governs the final morphology of the system. Matrix- or interface-located fillers usually produce a decrease in the particle diameter of the minor phase, being the increase in matrix viscosity[9–11] and the suppression of physical coalescence, respectively, the two main factors which contribute to condition the development of the morphology.[12–14] Dispersed phase-located fillers, on the other hand, can give rise to a "sea-island" to "co-continuous" morphological development in the system.[14–20] The reasons for this change are not entirely clear and further work is required to fully understand them. The increased viscosity[21] and the kinetically decreased mobility[14,22,23] of the filled minor phase can prevent the dispersed particles from fracturing during melt processing. In other systems, however, the self-agglomeration capacity of the fillers,[18,20,24] has been seen to lead to the morphological development of the system without affecting the main/minor phase viscosity ratio in any way. In any case, it is clear that main/minor phase compatibility plays a key role in the morphological development.[17]

From an applied point of view, the main reason for adding nanolayers to a polymer blend is to improve its mechanical and barrier properties. The nanolayers act as reinforcing agents[25] and, at the same time, as physical barriers against permeation.[26] As a good dispersion level of the nanolayer in the polymer matrix is essential, organically modified nanofillers are preferred instead of traditional unmodified ones, in order to improve compatibility between constituents.[27]

In the case of PLA/PCL blends, the specific goal is to compensate for the loss in stiffness[1] and gas-barrier performance[28] of PLA caused by the addition of PCL. Melt-processed PLA/PCL/OMMT nanocomposites[29–35] have already been characterized. Regarding the OMMT location, the nanolayers have appeared dispersed in the PLA-phase[29–31] or at the PLA/PCL interface[32] as a result of their higher affinity with PLA.[32] PLA/PCL/OMMT nanocomposites have shown an intercalated nanostructure,[29–35] and when OMMT located at the interface, it exfoliated.[32] Consequently, in PLA-rich compositions, the addition of OMMT has caused a decrease in the size of the PCL particles.[29,31,32,34] However, the morphology has evolved to co-continuity when PLA was the dispersed phase.[32]

In the present work, PLA/PCL/OMMT nanocomposites were obtained based on a compatible PLA/PCL 80/20 blend, and using a processing route that leads the nanofiller to locate in the thermodynamically less favored minor PCL phase. The nanostructure and the morphology of the nanocomposites was analyzed and related to the processing conditions employed. In addition, the viscoelastic, mechanical and barrier properties were measured and compared with those shown by reference PLA/OMMT nanocomposites processed under similar conditions.

EXPERIMENTAL

The PLA used was an injection molding grade NATUREWORKS 3052D (96% of L-lactide and density 1.24 g cm^{-3}), purchased from Resinex Spain S.L. The PCL was CAPA 6800 (M_w = 80,000 g mol^{-1}), purchased from Solvay. The organoclay was Cloisite 30B, a montmorillonite modified with a methyl tallow bis-2-hydroxyethyl quaternary ammonium salt; it was purchased from Southern Clay Products (Texas). The three components were dried to prevent any possible moisture-induced degradation from occurring during processing in the melt state.

All the compositions were melt-mixed in a Collin twin-screw extruder-kneader (type ZK25, *L*/*D* ratio = 30, screw diameter = 25 mm) at 180 °C. PLA/PCL/OMMT nanocomposites were melt-processed in two steps; first, the previously characterized[1] PLA/PCL 80/20 composition was obtained at 80 rpm and second, the PLA/PCL blend and the OMMT were mixed at 320 rpm. PLA/OMMT nanocomposites, prepared as reference materials, were also mixed at 320 rpm. In both the reference PLA/OMMT and PLA/PCL/OMMT nanocomposites, the 1.5, 3, 5, and 7% OMMT contents were set relative to the PLA content. Thus, the real OMMT contents in the ternary nanocomposites were 1.2, 2.5, 4.2, and 5.8%, respectively. The nanocomposites will be named PLA/PCL/x, where x is the nanofiller content with respect to the PLA. The PLA/PCL ratio was 80/20 in all cases. Obtained extrudates were pelletized and dried at 80 °C. PLA/PCL/3 nanocomposite pellets were further kneaded in a DSM MICRO 5 corotating twin-screw microextruder at 80 rpm and 180 °C, for 5, 10, and 15 min.

The pure PLA, the PLA/PCL 80/20 blend and the nanocomposites were injection-molded at 180 °C in a Battenfeld reciprocating screw-injection molding machine (type BA-230-E, *L*/*D* ratio = 17.8, screw diameter = 18 mm) to obtain tensile (ASTM D638 type IV, 3.2-mm thick) and impact (ASTM D256, 3.2-mm thick) specimens.

Extruded pellets were also compression-molded at 200 °C in a Collin PE-200 hot-pressing machine to obtain sheets in order to measure the viscoelastic and the oxygen-barrier properties of the nanocomposites. The machine was equipped with a water-circulating cooling system. The molding process was developed in three stages: preheating (closure without pressure) (3 min), compression (closure under 200 bar pressure) (2 min) and cooling under pressure (7 min).

The samples for transmission electron microscopy (TEM) were ultrathin-sectioned at 30–40 nm using an ultramicrotome. The micrographs were obtained in a Philips Tecnai 20 TEM at an accelerating voltage of 200 kV.

X-ray diffraction (XRD) was used to analyze the nanostructure and to determine the interlayer spacing between stacked OMMT platelets. XRD experiments were performed in a Philips PW 1729 GXRD diffractometer (wavelength, $\lambda = 0.15406$ nm). The diffraction spectra were recorded over a 2θ range of 0–10°. By ascertaining the incident and refracted angles, the basal spacing between adjacent OMMT sheets can be calculated using Bragg's law.

$$\lambda = 2\ d\ \sin\theta$$

where:

λ: Wavelength of the incident radiation
d: Basal spacing between OMMT sheets
θ: Angle between the incident or reflected radiation and the plane of the crystal.

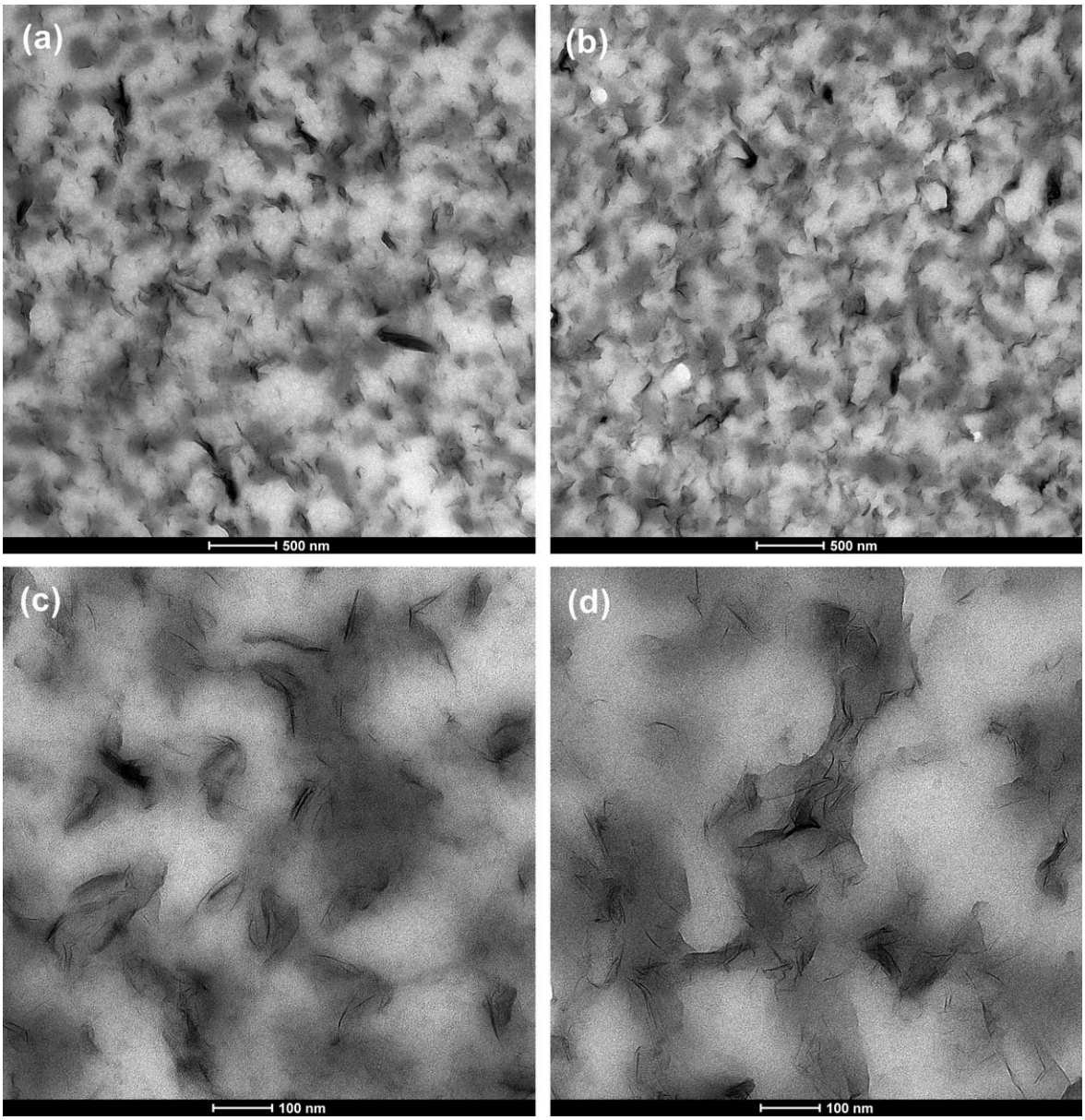

Figure 1. TEM micrographs of PLA/PCL/3 (a,c) and PLA/PCL/7 (b,d) nanocomposites taken at low (a,b) and high (c,d) magnifications.

The viscoelasticity tests were performed in an Anton Paar MCR 301 rheometer. Tests were carried out at a constant temperature of 180 °C under a nitrogen atmosphere using compression-molded specimens, with parallel plate geometry, 25 mm in diameter and 1-mm thick. In a first step, the linear viscoelastic region was determined for each studied material by varying the shear stress from 1 Pa to 1000 Pa at fixed frequencies of 1 rad s^{-1} and 100 rad s^{-1}. In a second step, the viscoelastic parameters were determined by spectromechanical analysis conducted in the area of linear viscoelasticity. The samples were subjected to a variable frequency between 100 and 0.01 rad s^{-1} at the previously fixed shear stress.

The interfacial tension (γ_{12}) between different OMMT/polymer pairs was estimated by using Wu's method[36] measuring the contact angle of two liquids on the surface of specimens of the different components using a CAM 100 goniometer (KSV). According to Wu's method:

$$\gamma_{12}=\gamma_1+\gamma_2+\frac{4\gamma_1^d\gamma_2^d}{\left(\gamma_1^d+\gamma_2^d\right)}+\frac{4\gamma_1^p\gamma_2^p}{\left(\gamma_1^p+\gamma_2^p\right)}$$

where subscripts 1 and 2 correspond to constituent 1 and constituent 2, respectively. Polar (γ^p), dispersive (γ^d) and total (γ) surface energies were determined from the corresponding contact angles of both constituents with water and ethylene glycol, respectively.

The phase structure was studied by DMTA analysis performed on a TA INSTRUMENTS DMA Q800 viscoelastometer that provided the plots of the storage (E') and loss (E'') modulus and loss tangent (tan δ) against temperature. The scans were carried out in single cantilever mode at a constant heating rate of

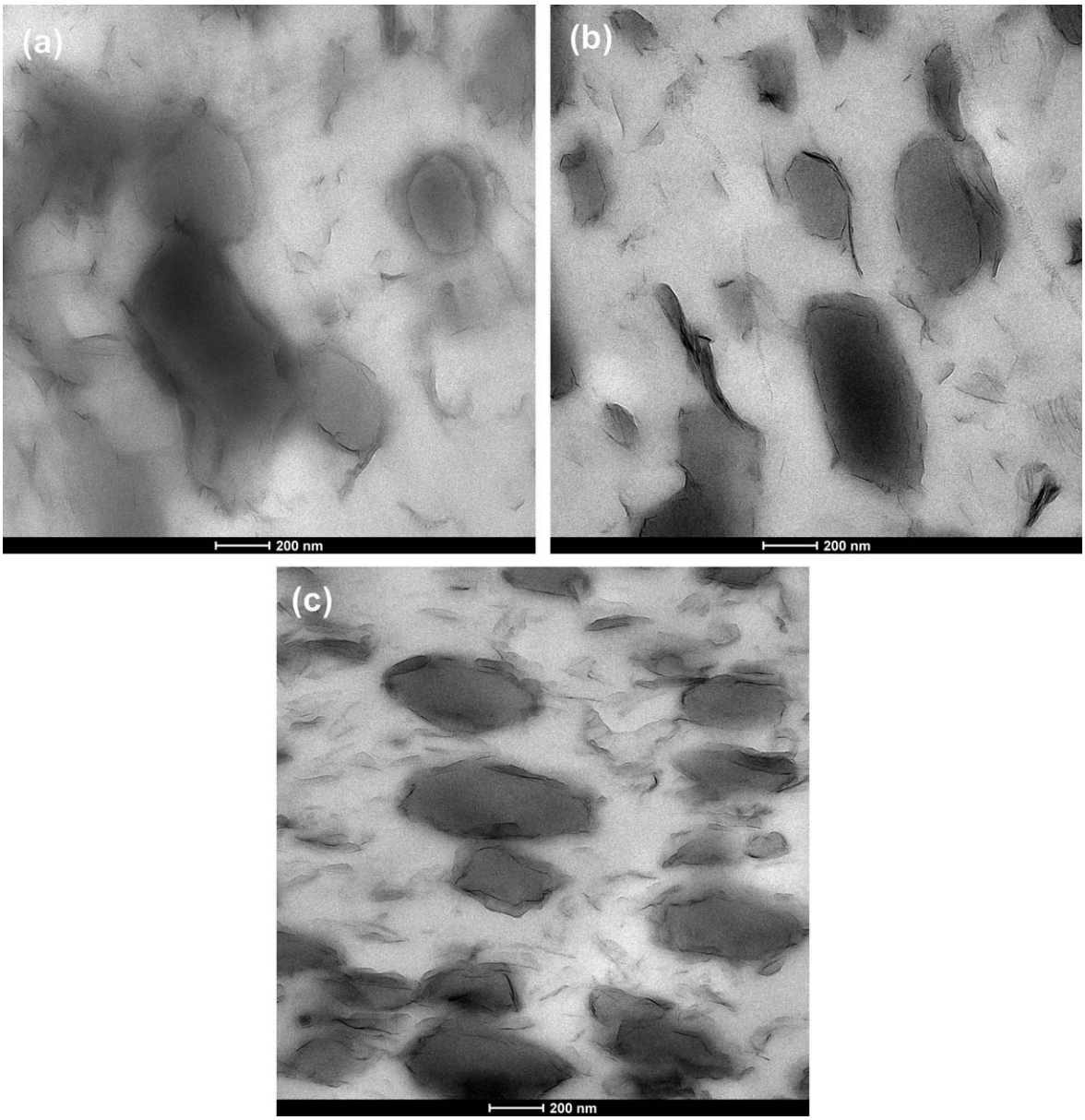

Figure 2. TEM micrographs of the PLA/PCL/3 nanocomposite after being remixed for 5 (a), 10 (b), and 15 (c) min in a recirculation microextruder.

4 °C min^{-1} and a constant frequency of 1 Hz. The PLA/PCL blend and PLA/PCL/OMMT ternary nanocomposites were analyzed between −100 and 100 °C.

The calorimetric analysis was performed by DSC using a Perkin Elmer DSC-7 calorimeter, calibrated with an Indium standard. The samples were heated from 30 to 200 °C at 20 °C min^{-1}. The melting (T_m) and cold crystallization (T_{cc}) temperatures of PLA and the melting temperature (T_m) of PCL were determined from the maxima of the corresponding peaks. Melting and crystallization enthalpies were determined from the area of each peak. The crystallization level of PLA was calculated using both enthalpies considering ΔH_f^{∞} of PLA is 93 J g^{-1}.[37] Although the melting peak of PCL was observed in all the compositions containing PCL, it was not possible to quantitatively calculate the crystallinity level because it overlapped with the glass transition of PLA.

Tensile tests were carried out using an Instron 4301 tensile tester. Young's modulus was determined at a cross-head speed of 1 mm min^{-1} by means of an extensometer, and the tensile strength and the elongation at break were measured at a cross-head speed of 10 mm min^{-1}. A minimum of five tensile specimens were tested for each reported value.

Izod Impact tests were carried out on notched specimens using a CEAST 6548/000 pendulum. The notches (depth = 2.54 mm and radius = 0.25 mm) were machined after injection molding. A minimum of eight specimens were tested for each reported value.

Oxygen permeation tests were carried out using a MOCON OX-TRAN MODEL 2/21 permeator and following the ISO 15105-1,2 standard, at 23 °C, with 0% relative humidity and at a pressure of 760 mm Hg.

RESULTS AND DISCUSSION

Nanostructure and Morphology: OMMT Location

Figure 1 shows TEM micrographs of PLA/PCL/3 (a,c) and PLA/PCL/7 (b,d) nanocomposites taken at low (a,b) and high (c,d) magnifications. The light continuous regions show the PLA phase, while the grey zones indicate the PCL phase, and the dark platelets are the OMMT. As can be observed, clay layers appeared mainly in the minor PCL phase and marginally at the PLA/PCL interphase. According to the interfacial tensions of the polymer/OMMT pairs determined from contact angle measurements (PLA/OMMT: 1.11 mN m^{-1} and PCL/OMMT: 2.9 mN m^{-1}), and consistent with previous results,[32] this indicates the location of clay layer in the thermodynamically less favored polymeric phase (PCL).

As described in the experimental part, the OMMT was added to a previously melt-processed PLA/PCL 80/20 blend in a second extrusion step. Furthermore, the melt-mixing conditions used to disperse the OMMT within the blend were based on high shear strain (screw-rotation speed: 320 rpm) and associated short residence times in the extruder (~30 s). These conditions are far from thermodynamic equilibrium conditions, where the location of the nanofillers is governed mainly by polymer/nanofiller interaction.[6] Under the used mixing conditions, the OMMT should initially connect with the PLA/PCL blend in the solid state. As the extrusion process proceeded, and the temperature of the material rose, the PCL melted to render a liquid material at a temperature (~60–65 °C) similar to the T_g of PLA, which softened to a rubbery state. Although PLA and PCL showed similar melt viscosities at 180 °C,[1] at these initial stages of the extrusion process and corresponding low temperatures, the rubbery PLA was much more viscous than the melted PCL. The high PLA/PCL viscosity ratio should kinetically favor the preferential location of the clay in the thermodynamically less favorable PCL phase. The short mixing times,[5] resulting from the high screw-rotation speed, prevented the OMMT from migrating to the more compatible PLA phase, and as a result, it remained in the less compatible PCL-phase at the end of processing.

To examine the proposed mechanism and the influence of the processing protocol used, extruded pellets of the PLA/PCL/3 composition were further mixed in a microextruder, operated in recirculation mode, at 180 °C and 80 rpm. Figure 2 shows TEM micrographs after remixing for 5 (a), 10 (b), and 15 (c) min. As can be seen, the location of the OMMT layers changed with respect to that shown in Figure 1(c). As the mixing time increased, increasing amounts of clay located in the light and more compatible PLA phase or at the PLA/PCL interphase [Figure 2(a–c)]. Moreover, the initial almost co-continuous morphology [Figure 1(c)] developed into a matrix-dispersed phase one [Figure 2(c)]. The PCL/OMMT-morphology relationship is discussed in detail in the following sections. The final resulting over-mixed morphology and OMMT dispersion and distribution is comparable to that observed by Wu *et al.*[32] for PLA/PCL/OMMT nanocomposites blended in an internal mixer for 6 min at 80 rpm.

Morphology

With respect to the morphology of the PCL dispersed phase, Figure 3 shows that of the reference unfilled 80/20 blend. When

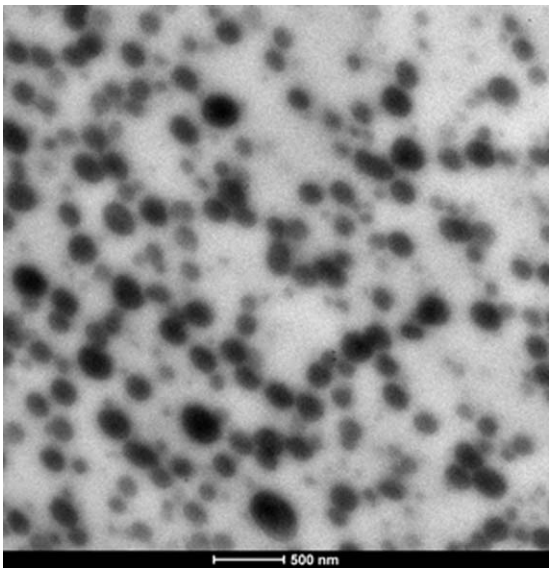

Figure 3. TEM micrograph of the PLA/PCL 80/20 blend.

compared with the morphology of the ternary PLA/PCL/OMMT nanocomposites of Figure 1, it can be seen that the presence of the OMMT nanoplatelets in the PCL phase led to a change in the shape of this phase. The "sea-island" morphology of the PLA/PCL blend, in which submicron PCL particles appeared finely dispersed within the PLA,[1] evolved towards a co-continuous morphology. The presence of clay in the dispersed PCL phase is known to increase its viscosity[38] so that the weaker mastication caused by the PLA matrix was not able to fracture these PCL domains but did cause them to deform and eventually elongate. This argument also supports the previously mentioned "reversion" of the PLA/PCL/3 nanocomposite to a "sea-island" morphology [Figure 2(c)] when, upon further kneading, OMMT particles migrated from the PCL- to the PLA-phase.

Nanostructure

With respect to the OMMT platelets, they showed an intercalated/exfoliated nanostructure within the PCL (Figure 1), and both the number and size of the OMMT stacks increased when the amount of OMMT was increased. In any case, the overall dispersion of the OMMT remained good even at the highest OMMT content [Figure 1(b,d)]. The OMMT intercalation was confirmed by analyzing the XRD diffraction patterns of the nanocomposites, which are plotted in Figure 4 together with those of the reference binary PLA/3 and PLA/7 ones.

The OMMT interlaminar distance was close to 3.16 nm, so the Δd_{001} with respect to the pure OMMT (1.85 nm[39]) was close to 1.3 nm. Similar interlaminar distances have also been reported in previous high shear-strain extruded PCL/Cloisite 30 B nanocomposites.[39] This interlaminar distance of PLA/PCL/OMMT nanocomposites was almost the same as that estimated for the reference PLA/OMMT ones, as can be observed in Figure 4. This indicates that the Δd_{001} was independent of whether the OMMT was located in the PLA phase in binary nanocomposites or in the PCL phase in ternary nanocomposites.

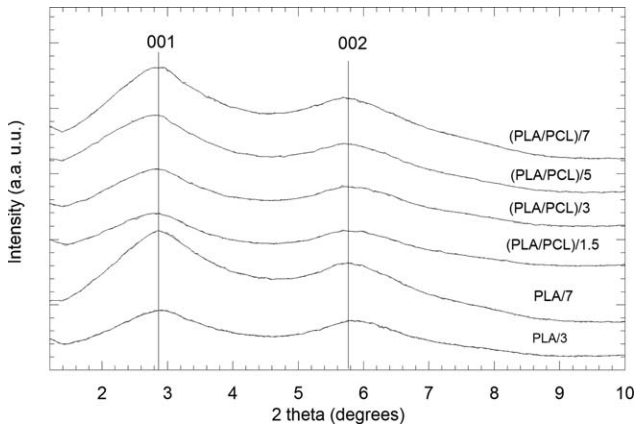

Figure 4. XRD diffractograms of reference PLA/OMMT and ternary PLA/PCL/OMMT nanocomposites.

Viscoelasticity

Figure 5 shows the storage modulus (G') vs. angular frequency (ω) plots of the PLA/PCL/OMMT nanocomposites (unfilled symbols) and reference PLA/OMMT nanocomposites (filled symbols). As can be seen, the viscoelastic behavior of the PLA/PCL/OMMT nanocomposites was dominated by the liquid-like behavior of the PLA/PCL blend[40] up to the PLA/PCL/5 composition. Broad relaxations between 0.01 and 10 rad s^{-1} and increasing G' values at increasing OMMT contents, associated with the presence of OMMT,[41] were observed in these compositions. However, the PLA/PCL/7 composition, in contrast, showed a typical solid-like behavior, indicating structural percolation of the organoclay within the polymer blend.

The overall viscoelastic behavior of the reference PLA/OMMT nanocomposites, with the OMMT percolating at the PLA/7 composition, was very similar. The only noticeable difference was the higher G' values of the PLA/PCL/OMMT nanocomposites, resulting from the higher G' value of the PLA/PCL blend with respect to that of pure PLA.

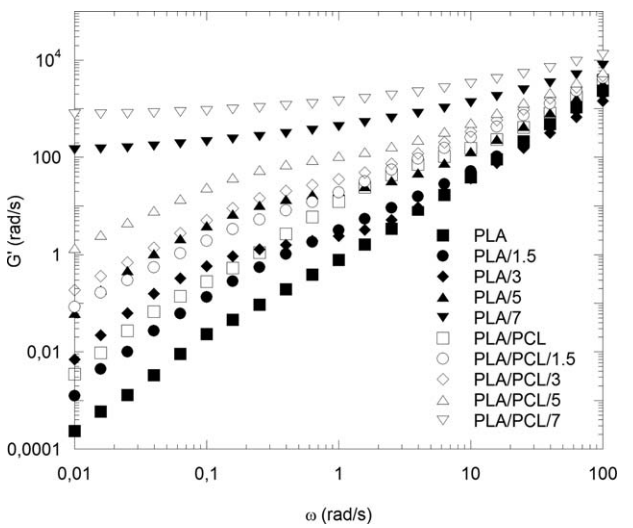

Figure 5. G' vs. ω plots of the PLA/PCL 80/20 blend and of the PLA/OMMT and PLA/PCL/OMMT nanocomposites.

The viscoelastic behavior in polymer nanocomposites is directly related to the dispersion level of the nanofiller.[42] Thus, the results in Figure 5, which are consistent with the similar OMMT interlaminar distances deduced from XRD tests (Figure 4), indicate a similar OMMT dispersion level in both pure PLA and in the PLA/PCL blend, regardless of whether it was PLA or PCL-located, respectively. Therefore, the high shear-strain mixing conditions employed not only led to the non-thermodynamic OMMT-location in PLA/PCL/OMMT nanocomposites, but also to a dispersion level similar to that of pure PLA.

It has been reported that a relationship exists between the morphology of a biphasic system and the G' slope in the low-frequency flowing zone.[43–45] Even if the results are not fully conclusive, the slope of co-continuous systems is usually lower than that observed in sea-island type systems. In Figure 5, the slope of the G' vs. ω plot in the flowing zone remained close to 2 in non-percolated PLA/OMMT nanocomposites, whereas in the case of PLA/PCL/OMMT nanocomposites, it dropped from 2 (unfilled PLA/PCL blend) to 1.4 or less, even at the lowest OMMT content. Although the results are not fully conclusive, according to the aforementioned literature, they provide additional evidence of the previously proposed morphological changes from the PLA/PCL blend to the PLA/PCL/OMMT nanocomposites.

To offer some insight into the morphological evolution of PLA/PCL/OMMT nanocomposites with OMMT content, Figure 6(a,b) show the η^* vs. ω and tan δ vs. ω plots, respectively. The complex viscosity behavior of both PLA/7 and PLA/PCL/7 nanocomposites was typical of percolated systems, with the η^* values sharply rising at low frequencies. The behavior of the PLA/PCL/5 nanocomposite was different to that of the percolated compositions, but, the η^* values at low frequencies increased and were significantly higher than those of all the other non-percolated compositions. This behavior has been reported as characteristic for co-continuous structures.[43,44] Similarly, the shape of the tan δ vs. ω plot of the PLA/PCL/5 composition at very low frequencies, very similar to the almost flat plot of the percolated PLA/PCL/7, has been reported[46] as typical of polymer blends showing co-continuous morphologies. This is because the characteristic relaxation times required for interconnected big domains are very different from those required for the drops shown in sea-island morphologies.[46]

So, it can be concluded that the PLA/PCL/5 composition behaved as a partially co-continuous system. The behavior of the non-percolated PLA/PCL/1.5 and PLA/PCL/3 compositions was also different to that of the PLA/PCL blend, and also to that of the nonpercolated PLA/OMMT nanocomposites with respect to pure PLA. These small differences are also most probably related to the morphological evolution of the PLA/PCL system.

Phase Structure

Figure 7 shows tan δ vs. temperature plots of the 80/20 PLA/PCL blend[1] and those of the PLA/PCL/3 and PLA/PCL/7 nanocomposites obtained by DMTA. Two tan δ signals,

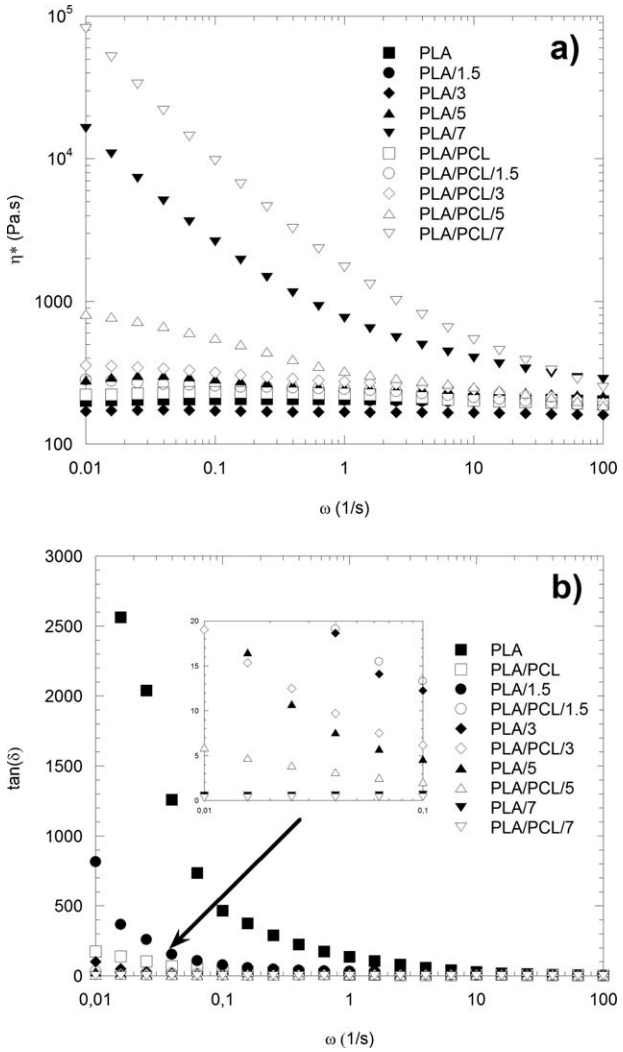

Figure 6. Complex viscosity (η*) vs. ω (a) and tan δ vs. ω (b) plots of PLA/OMMT and PLA/PCL/OMMT nanocomposites.

corresponding to the α-transitions of PLA and PCL were observed both in the unfilled blend and in the ternary nanocomposites. As can be seen in Figure 7, the position of the PCL peak remained close to −45 °C in all cases. The temperature of the PLA peak in the nanocomposites was slightly higher than the value of the unfilled 80/20 blend (61.2 °C), but the variations observed remained close to the experimental error of the measurement. This indicates that the presence of OMMT did not modify the immiscibility of the PLA/PCL[1] blend in agreement with previous results on PLA/PCL/OMMT nanocomposites.[29,32] In fact, only on rare occasions and when located at the interface, have nanofillers been found to partially[47–50] or even fully[49,50] miscibilize immiscible polymer blends.

Figure 8 shows the DSC plots of the first heating scans of the PLA/PCL blend and the PLA/PCL/3 and PLA/PCL/7 nanocomposites. Two endothermic and one exothermic transitions were observed in all the compositions. The low temperature endothermic transition reflects the melting of PCL, while the high temperature transition reflects the melting of PLA. The exothermic transition represents the cold crystallization of PLA.

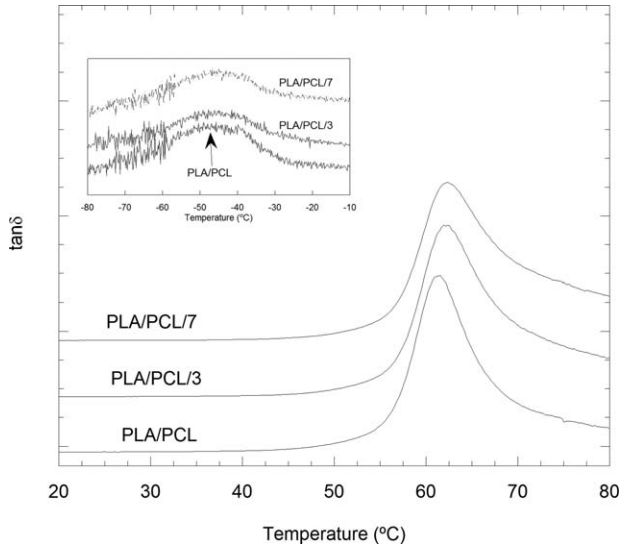

Figure 7. Tan δ vs. temperature plots of the PLA/PCL 80/20 blend and of the PLA/PCL/3 and PLA/PCL/7 nanocomposites from 20 to 80 °C and from −80 to −10 °C.

Table I shows DSC data for all the compositions. Both the melting temperature and the degree of crystallinity of PLA almost remained within the experimental error of the measurement in the presence of OMMT. The small variations observed were hardly significant and, furthermore, did not reveal any clear trend.

The cold crystallization temperature of PLA varied depending on the OMMT content in a complex way, probably due to the combined effect of both PCL and OMMT. However, the variations observed did not affect the melting behavior of PLA, indicating that the amount and the perfection of the PLA-crystals created was similar in all cases. Both the melting temperature (Table I) and the melting enthalpy of PCL (Figure 8) decreased at increasing OMMT contents. These results are consistent with

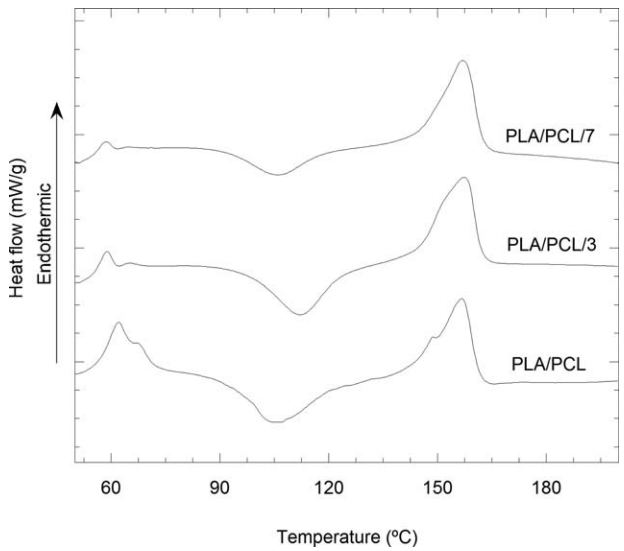

Figure 8. The first DSC heating scans of the 80/20 PLA/PCL blend and of the PLA/PCL/3 and PLA/PCL/7 nanocomposites.

Table I. The Melting Temperatures of PLA (T_{mPLA}) and PCL (T_{mPCL}) and Degrees of Crystallinity of PLA (X_{cPLA}) in the PLA/PCL/OMMT Nanocomposites

Composition	T_{mPLA} (°C)	T_{mPCL} (°C)	X_{cPLA} (%)
PLA/PCL[a]	156.7	62.0	4.8
PLA/PCL/1.5	159.4	61.7	4.6
PLA/PCL/3	158.7	59.4	7.5
PLA/PCL/5	157.4	58.7	4.9
PLA/PCL/7	157	58.3	9.8

[a] Values from Ref. 1.

the literature,[51] and indicate that OMMT hindered the ability of the PCL to crystallize.

Mechanical Properties

Figure 9 shows the Young's modulus values for the reference PLA/OMMT and the PLA/PCL/OMMT nanocomposites vs. the true OMMT content. The stress/strain curves of the ternary nanocomposites have also been included. As can be seen, Young's modulus of the PLA/PCL blend increased with the OMMT content as a result of the reinforcing effect produced by the organoclay. The increase was linear in the OMMT content range studied. The addition of OMMT was very efficient and helped to recover the loss of stiffness (about 15.5%) caused by the PCL in the PLA. The Young's modulus values of the PLA/PCL/1.5 and PLA/PCL/3 nanocomposites were 3350 ± 120 MPa and 3470 ± 70 MPa, respectively, close to that of pure PLA, 3520 ± 20 MPa. The maximum Young's modulus obtained, which was for the PLA/PCL/7 composition, was 3940 ± 90 MPa, 12% higher than that of pure PLA, and 29% higher than that of the reference 80/20 blend.

The reinforcing effect of the OMMT in the PLA/PCL blend was similar to that of the neat PLA, since Figure 9 shows similar relative modulus increases in the PLA/OMMT and ternary PLA/PCL/OMMT nanocomposites. These results indicate that the reinforcing ability of the OMMT in this study was similar regardless of whether it was located within the main matrix phase (PLA/OMMT) or within the minor dispersed phase (PLA/PCL/OMMT). These findings are consistent with those

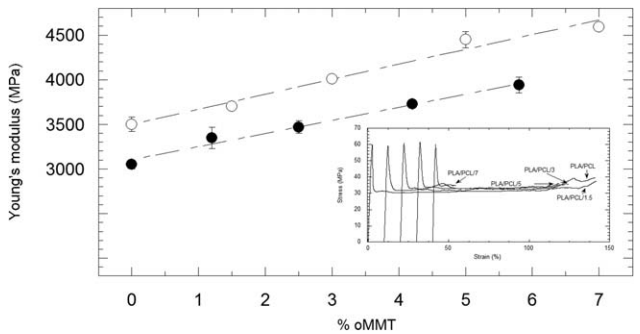

Figure 9. The Young's modulus values of PLA/OMMT (○) and PLA/PCL/OMMT (●) nanocomposites with respect to the OMMT content. Stress-strain curves of PLA/PCL/OMMT nanocomposites are included in the figure. Curves have been displaced in the horizontal axis for a better clarity.

observed in PA6/elastomer/OMMT nanocomposites,[8] where the reinforcing effect of the OMMT was also similar irrespective of its matrix- or dispersed phase-location. The good dispersion and similar intercalation level shown by the OMMT in both the binary and ternary systems of this work is also consistent with these results.

Existing literature on the mechanical properties of ternary PLA/PCL/OMMT nanocomposites is scarce. Li *et al.*[33] studied the effect of adding unmodified and modified Cloisite 25A to a PLA/PCL blend, where the composition is not mentioned. It can be deduced that the PCL content must have been high, because the Young's modulus and yield strength values of the unreinforced PLA/PCL blend were very low (1120 and 40 MPa, respectively). The Young's modulus increases in the nanocomposites were significant, even higher than those reported in this work (40% at 5% OMMT). Moreover, when the modified organoclay was used, the results were even better (47% at the same OMMT content) but, given the very low initial value of the unreinforced PLA/PCL blend, the maximum value obtained was 50% lower than the maximum recorded in this study. In the work of Yu *et al.*,[29] significant increases in Young's modulus (19.5 and 23% with 1 and 3% Nanocor I.34 OMMT contents, respectively) were followed by even greater and unexplained decreases as the OMMT content increased (up to 10% OMMT content) when added to a 90/10 PLA/PCL blend. As in the work of Li *et al.*[33] the initial modulus value of the unreinforced PLA/PCL blend was surprisingly low (1950 MPa).

The behavior of the tensile strength of the PLA/PCL/OMMT nanocomposites in this study was also favorable, remaining similar to that of the unreinforced PLA/PCL blend (60.3 MPa) (variations smaller than the standard deviation). Significant decreases in tensile strength have been observed at high OMMT contents in previously studied PLA/PCL/OMMT nanocomposites[29,31] and only marginal increases at low OMMT contents,[29,31] or in the whole OMMT content range when the clay was modified,[33] have been reported. The behavior observed in PLA/PCL/OMMT nanocomposites of this work was similar to that observed in the reference PLA/OMMT nanocomposites, probably related to the similar dispersion of OMMT in the binary and ternary nanocomposites.

Figure 10 shows the ductility (measured as the elongation at break) with respect to the true OMMT content in PLA/PCL/OMMT nanocomposites. As can be seen, the elongation at break of the PLA/PCL blend decreased with the OMMT content. However, it was higher than 100% in PLA/PCL/1.5 and PLA/PCL/3 nanocomposites, and stayed close to 80% even in the PLA/PCL/5 composition. Only the PLA/PCL/7 composition showed close-to-brittle behavior, probably related to the structural percolation of the organoclay, previously referred to in this article. These results are clearly more favorable than those reported in the literature for systems of this kind, where the elongation at break decreased by 63% with 2% OMMT and by 78% with 5% OMMT, respectively, even in the most favorable case (modified OMMT),[33] or sharply decreased to brittle values.[29]

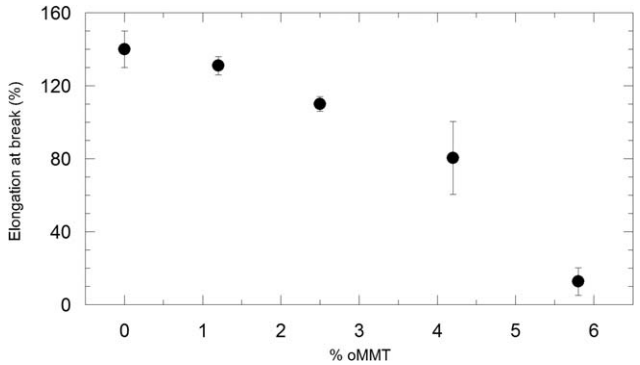

Figure 10. The elongation at break of PLA/PCL/OMMT nanocomposites with respect to the OMMT content.

The high ductility of the nanocomposites in this study indicates that, in the presence of OMMT, PCL partially maintained its ductile behavior in PLA/PCL/OMMT nanocomposites, at least up to the PLA/PCL/5 composition. This result is consistent with the bibliography,[52] where highly deformable PCL/OMMT nanocomposites (elongation at break up to 500%) have been obtained at OMMT contents as high as 4%. Moreover, it has also been reported that efficient stress transfer between polymeric phases[53] is still possible when the interphase is not saturated with OMMT.

Figure 11 shows that the impact strength of the PLA/PCL/OMMT nanocomposites also decreased at increasing OMMT contents and behaved less positively than the elongation at break. No impact strength data for PLA/PCL/OMMT nanocomposites have been found in the literature, except for a PLA/poly(ε-caprolactone-*co*-lactide) copolyester blend filled with silica nanofillers, where supertough materials were obtained at high filler contents. This was related to the favorable initial behavior of the unfilled blend and to the almost continuous morphology developed in the presence of the nanofiller.[54]

Oxygen Permeability

Figure 12 shows the oxygen permeability of PLA/OMMT and PLA/PCL/oMMT nanocomposites with respect to the real OMMT content. The continuous line shows the permeability of pure PLA. As can be seen, the permeability of the PLA/PCL 80/20 blend was significantly higher (0.37 Barrer) than that of pure PLA (0.29 Barrer), as a result of the higher permeability of PCL

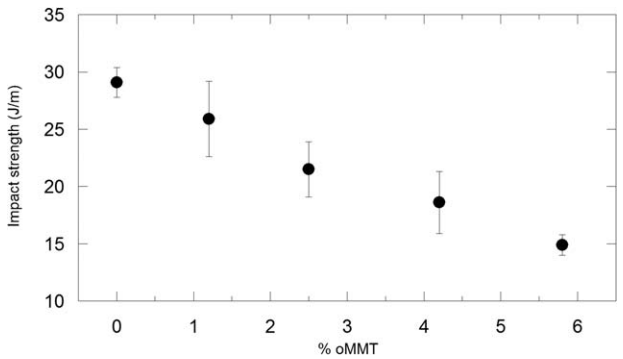

Figure 11. The notched Izod impact strength of PLA/PCL/OMMT nanocomposites with respect to the OMMT content.

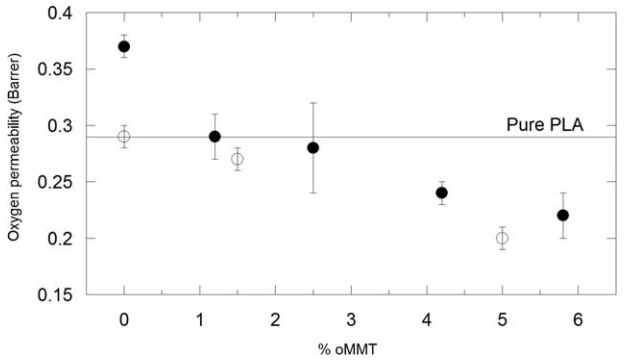

Figure 12. The oxygen permeability values of PLA/OMMT (○) and PLA/PCL/OMMT (●) nanocomposites with respect to the OMMT content. The continuous line indicates the oxygen permeability of pure PLA.

(0.90 Barrer). According to the morphology of the PLA/PCL blend (Figure 3), during permeation through the PLA matrix, O_2 molecules find finely and homogeneously distributed PCL dominions, thus facilitating easier and faster diffusion through the blend.

Figure 12 also shows that the addition of OMMT in ternary nanocomposites led to a decrease in permeability. The decrease was sharp at low OMMT contents and slower at higher OMMT contents. When this behavior is compared to that observed in the reference binary PLA/OMMT nanocomposites, it can be seen that the decreases in permeability in the PLA/PCL blend were significantly greater (21 and 35% with 1.5 and 5% OMMT, respectively) than in the pure PLA (7 and 31%, respectively), even when the true overall OMMT content was lower in the former than in the latter.

Two factors need to be considered when analyzing the effect of adding OMMT to PLA and PLA/PCL: (1) the nanoplatelets themselves and (2) the preferential location of the nanofiller in PLA and in the PCL phase and the ensuing change in morphology. The presence of nanoplatelets is common in both PLA/OMMT and PLA/PCL/OMMT nanocomposites, so the second factor must be responsible for the enhanced barrier behavior of the latter. This is because the preferential location of the OMMT in the PCL phase counteracts the higher permeability of this polymer with respect to pure PLA and, moreover, the transition to co-continuous morphologies caused by the OMMT would also help to prevent the O_2 molecules from finding a continuous path through the PLA matrix.

Finally, and as can be seen in Figure 12, permeability values similar or even lower than those of pure PLA can be obtained at intermediate OMMT contents. This behavior, along with the very favorable mechanical performance described in the previous section (Young's modulus similar to that of pure PLA, high strength and ductility) makes these materials very attractive potential candidates for practical applications.

CONCLUSIONS

PLA/PCL/OMMT nanocomposites with different OMMT contents were melt-processed in a twin screw-extruder under high shear and low residence time mixing conditions. The PLA/PCL

ratio was fixed at 80/20. These conditions induced a mainly PCL-location of the organoclay, although the nanofiller was thermodynamically more compatible with the main PLA phase. Furthermore, and as a result of this minor phase-location, the morphology of the system evolved from "sea-island" to "co-continuous." This morphological evolution was analyzed in depth using viscoelastic measurements, which indicated that the system started to behave as a co-continuous system above and beyond a 5% OMMT content. The OMMT showed an intercalated/exfoliated nanostructure within the minor PCL phase. The calculated OMMT interlaminar distance showed a $\Delta d_{001} = 1.3$ nm with respect to that of pure OMMT, and coincided with the OMMT interlaminar distance in PLA/OMMT nanocomposites. Moreover, the G' vs. ω behavior of PLA/OMMT and PLA/PCL/OMMT nanocomposites was very similar. These results suggest a similar OMMT dispersion level within pure PLA and the PLA/PCL blend despite its different location. The effect of the presence of OMMT in the PLA/PCL blend was very noticeable in its macroscopic properties. The stiffness of the nanocomposites increased linearly with the amount of OMMT present, and, at OMMT contents of over 3%, the modulus of the ternary nanocomposites was comparable or higher than that of the pure PLA. The elongation at break of the blend decreased with the OMMT content but the highly ductile behavior of the system remained up to the PLA/PCL/5 composition. Finally, the addition of OMMT produced a noticeable decrease in the oxygen permeability of the blend, all the ternary nanocomposites showing similar or better barrier behavior than the pure PLA.

ACKNOWLEDGMENTS

The financial support of the Basque Government (project IT611-13) and of the University of the Basque Country (UFI 11/56) is gratefully acknowledged. J. Urquijo also acknowledges the Spanish MINECO for the award of a grant for the development of this study.

REFERENCES

1. Urquijo, J.; Guerrica-Echevarria, G.; Eguiazabal, J. I. *J. Appl. Polym. Sci.* **2015**, *132*, 42641.
2. Semba, T.; Kitagawa, K.; Ishiaku, U. S.; Hamada, H. *J. Appl. Polym. Sci.* **2006**, *101*, 1816.
3. Takayama, T.; Todo, M.; Tsuji, H.; Arakawa, K. *J. Mater. Sci.* **2006**, *41*, 6501.
4. Harada, M.; Iida, K.; Okamoto, K.; Hayashi, H.; Hirano, K. *Polym. Eng. Sci.* **2008**, *48*, 1359.
5. Fenouillot, F.; Cassagnau, P.; Majeste, J. C. *Polymer* **2009**, *50*, 1333.
6. Taguet, A.; Cassagnau, P.; Lopez-Cuesta, J. M. *Prog. Polym. Sci.* **2014**, *39*, 1526.
7. Dasari, A.; Yu, Z. Z.; Mai, Y. W. *Polymer* **2005**, *46*, 5986.
8. Gallego, R.; García-López, D.; López-Quintana, S.; Gobernado-Mitre, I.; Merino, J. C.; Pastor, J. M. *J. Appl. Polym. Sci.* **2008**, *109*, 1556.
9. Li, Y. J.; Shimizu, H. *Polymer* **2004**, *45*, 7381.
10. Tiwari, R. R.; Paul, D. R. *Polymer* **2011**, *52*, 1141.
11. Tiwari, R. R.; Paul, D. R. *Polymer* **2011**, *52*, 4955.
12. Mishra, J. K.; Chang, Y. W.; Choi, N. S. *Polym. Eng. Sci.* **2007**, *47*, 863.
13. Khatua, B. B.; Lee, D. J.; Kim, H. Y.; Kim, J. K. *Macromolecules* **2004**, *37*, 2454.
14. Filippone, G.; Dintcheva, N. T.; La Mantia, F. P.; Acierno, D. *Polymer* **2010**, *51*, 3956.
15. Zou, H.; Wang, K.; Zhang, Q.; Fu, Q. *Polymer* **2006**, *47*, 7821.
16. Filippone, G.; Idintcheva, N. T.; La Mantia, F. P.; Acierno, D. *J. Polym. Sci. B: Polym. Phys.* **2010**, *48*, 600.
17. Nuzzo, A.; Bilotti, E.; Peijs, T.; Acierno, D.; Filippone, G. *Polymer* **2014**, *55*, 4908.
18. Cai, X.; Li, B.; Pan, Y.; Wu, G. *Polymer* **2012**, *53*, 259.
19. Xiu, H.; Zhou, Y.; Dai, J.; Huang, C.; Bai, H.; Zhang, Q.; Fu, Q. *RSC Adv.* **2014**, *4*, 37193.
20. Wu, G.; Li, B.; Jiang, J. *Polymer* **2010**, *51*, 2077.
21. Wang, L.; Shi, C.; Guo, Z. X.; Yu, J. *J. Ind. Eng. Chem.* **2014**, *20*, 259.
22. Steinmann, S.; Gronski, W.; Friedrich, C. *Polymer* **2002**, *43*, 4467.
23. Li, L.; Miesch, C.; Sudeep, P. K.; Balazs, A. C.; Emrick, T.; Russell, T. P.; Hayward, R. C. *Nano Lett.* **2011**, *11*, 1997.
24. Xiang, F.; Shi, Y.; Li, X.; Huang, T.; Chen, C.; Peng, Y.; Wang, Y. *Eur. Polym. J.* **2012**, *48*, 350.
25. Chan, M. L.; Lau, K. T.; Wong, T. T.; Ho, M. P.; Hui, D. *Comp. B Eng.* **2011**, *42*, 1708.
26. Choudalakis, G.; Gotsis, A. D. *Eur. Polym. J.* **2009**, *45*, 967.
27. Pinnavaia, T. J.; Beall, G. W. *Polymer–Clay Nanocomposites*; Wiley, New York, **2000**; Chapter 5, p 99.
28. Cabedo, L.; Feijoo, J. L.; Villanueva, M. P.; Lagaron, J. M.; Gimenez, E. *Macromol. Symp.* **2006**, *233*, 191.
29. Yu, Z.; Yin, J.; Yan, S.; Xie, Y.; Ma, J.; Chen, X. *Polymer* **2007**, *48*, 6439.
30. Ren, J.; Yu, T.; Li, H.; Ren, T.; Yang, S. *Polym. Compos.* **2008**, *29*, 1145.
31. Hoidy, W. H.; Al-Mulla, E. A. J.; Al-Janabi, K. W. *J. Polym. Environ.* **2010**, *18*, 608.
32. Wu, D.; Lin, D.; Zhang, J.; Zhou, W.; Zhang, M.; Zhang, Y.; Wang, D.; Lin, B. *Macromol. Chem. Phys.* **2011**, *212*, 613.
33. Li, Q.; Yoon, J. S.; Chen, G. X. *J. Polym. Environ.* **2011**, *19*, 59.
34. Shafiei, S. S.; Katbab, A. A. *J. Appl. Polym. Sci.* **2009**, *111*, 1954.
35. Hoidy, W. H.; Ahmad, M. B.; Jaffar, A. E. A.; Ibrahim, N. A. B. *J. Appl. Sci.* **2010**, *10*, 97.
36. Wu, S. J. Polymer Interfaces and Adhesion; Marcel Dekker, New York, **1982**; Chapter 8, p 266.
37. Wu, D. F.; Wu, L.; Zhang, M.; Zhao, Y. L. *Polym. Degrad. Stabil.* **2008**, *93*, 1577.
38. Di, Y. W.; Iannace, S.; Di Maio, E.; Nicolais, L. *J. Polym. Sci. B: Polym. Phys.* **2003**, *41*, 670.

39. Labidi, S.; Azema, N.; Perrin, D.; Lopez-Cuesta, J. M. *Polym. Degrad. Stabil.* **2010**, *95*, 382.
40. Chafidz, A.; Ali, M. A.; Elleithy, R. *J. Mater. Sci.* **2011**, *46*, 6075.
41. Hassanabadi, H. M.; Wilhelm, M.; Rodrigue, D. *Rheol. Acta* **2014**, *53*, 869.
42. Ray, S. S.; Okamoto, M. *Prog. Polym. Sci.* **2003**, *28*, 1539.
43. Steinmann, S.; Gronski, W.; Friedrich, C. *Rheol. Acta* **2002**, *41*, 77.
44. Potschke, P.; Paul, D. R. *Macromol. Symp.* **2003**, *198*, 69.
45. Yu, W.; Zhou, W.; Zhou, C. *Polymer* **2010**, *51*, 2091.
46. Li, R.; Yu, W.; Zhou, C. *J. Macromol. Sci. B: Phys.* **2006**, *45*, 889.
47. DePolo, W. S.; Baird, D. G. *Polym. Compos.* **2009**, *30*, 200.
48. Wu, D.; Zhang, Y.; Zhang, M.; Yu, W. *Biomacromolecules* **2009**, *10*, 417.
49. Ray, S. S.; Bousmina, M.; Maazouz, A. *Polym. Eng. Sci.* **2006**, *46*, 1121.
50. Voulgaris, D.; Petridis, D. *Polymer* **2002**, *43*, 2213.
51. Lepoittevin, B.; Devalckenaere, M.; Pantoustier, N.; Alexandre, M.; Kubies, D.; Calberg, C.; Jerome, R.; Dubois, P. *Polymer* **2002**, *43*, 4017.
52. Pantoustier, N.; Lepoittevin, B.; Alexandre, M.; Kubies, D.; Calberg, C.; Jerome, R.; Dubois, P. *Polym. Eng. Sci.* **2002**, *42*, 1928.
53. Goitisolo, I.; Gonzalez, I.; Eguiazabal, J. I. *J. Polym. Adv. Technol.* **2013**, *24*, 357.
54. Odent, J.; Habibi, Y.; Raquez, J. M.; Dubois, P. *Comp. Sci. Tech.* **2013**, *84*, 86.
55. Paul, M. A.; Alexandre, M.; Degee, P.; Henrist, C.; Rulmont, A.; Dubois, P. *Polymer* **2003**, *44*, 443.